New Design Rules and Experimental Study of Slightly Flared 1480-nm Pump Lasers

Ali Guermache, Vincent Voiriot, Rose-Marie Capella, Philippe Gallion, and Joël Jacquet

***Abstract*—Slightly flared lasers are investigated in order to minimize the longitudinal spatial hole burning impact on the output power saturation of 1480-nm pump lasers. In such a device, the stripe width is narrow at the rear facet for strong single lateral mode operation whereas at the front facet the stripe widens in order to reduce the photon density and as a consequence decrease gain saturation through hole burning effect. We proposed a slightly flared lasers design in order to maintain a uniform photon density along the active stripe. Experimentally, this novel structure exhibits single transverse-mode operation and a 30% output power improvement is obtained compared to the straight active waveguide.**

***Index Terms*—Flared waveguide, high-power semiconductor lasers, spatial hole burning.**

I. Introduction

THE GROWTH in wavelength-division-multiplexing systems requires high output power single transverse-mode laser diodes for Raman and erbium-doped fiber amplifier pump sources. Several approaches have shown high output powers emission [1]–[3]. In these papers, the design rules are mainly related to the active volume increase through large [1] or flared [2] waveguides or the use of multimode interferometer [3]. Such designs lead to electrical and thermal resistance decrease. Flared waveguides have been initially proposed and demonstrated for 980-nm pump lasers in order to reduce photon density close to the antireflection coating facet and as a consequence to limit the catastrophic optical mirror damage at high output power [4], [5]. Spatial hole burning reduction in such waveguides has been mentioned to be the origin of a better resistance against kink or beam steering [6].

In this work, we propose new design rules that allow us to define the waveguide width profile with respect to longitudinal spatial hole burning (LSHB) reduction. The design principle of the structure is based on the use of a uniform photon density along the cavity for a given current. The letter is organized as follows: In Section II, the concept of the structure is given and calculations allowing designing the flared waveguide are presented. The fabrication of the device is depicted in Section III. Finally, the results are given and discussed in Section IV for design structures optimized at two different currents.

II. Flared Concept

Rinner *et al.* [7] have demonstrated that a straight laser with antireflection and high-reflection coated facets provide a nonuniform photon density, leading to an inhomogeneous carrier density distribution along the active stripe. In such straight structure, close to the low reflectivity facet, the photon density is found to be high and the carrier density low. This leads to gain saturation at high power. This gain saturation has been demonstrated to be the origin of power saturation at high current injection. One way to limit this saturation is the use of flared structures that allow obtaining more uniform carrier and photon densities along the cavity [8]. We propose, in the following, to give the design rules for slightly flared cavity waveguides that compensate for the LSHB effect in 1480-nm pump lasers in order to enhance their output power.

In the first step, we calculate the photon density profile in a straight waveguide. Using a one-dimensional model [9], based on the transfer matrix method [10], the photon $S(z)$ and carrier $N(z)$ densities along the cavity laser are calculated at threshold and above threshold by solving the general rate equation for the photon and the carrier densities

$$\frac{dN}{dt} = \frac{J}{ed} - (A_{nr}N + B_rN^2 + C_{nr}N^3) - v_g g(N)S \quad (1)$$

$$\frac{dS}{dt} = v_g g(N)S - v_g(\alpha_i + \alpha_m)S + \beta B_r N^2 \quad (2)$$

where N is the carrier density, S the photon density, J the bias current density, $g(N)$ the gain material, e the electronic charge, d the active layer thickness, v_g the group velocity, β the spontaneous emission coefficient, and α_i and α_m are the internal and mirror losses, respectively; A_{nr}, the nonradiative recombination coefficient, B_r, the bimolecular spontaneous coefficient, and C_{nr}, the Auger recombination, are related to the carrier consumption mechanism.

Taking into account the LSHB effect, calculations of the photon $S(z)$ and carrier $N(z)$ density profiles, in a 1500-μm-long straight laser, were carried out for different currents at $I \cong I_{\mathrm{threshold}}$ and $I \cong 25 I_{\mathrm{threshold}}$ [see Fig. 1(a) and (b)], respectively. The front and reverse facet reflectivities are assumed to be 3% and 95%, respectively.

As expected, calculations clearly predict a nonuniform photon density along the cavity with a continuous increase of $S(z)$ from the back to the front facet. It is worth noting the difference in the concavity of $S(z)$ between Fig. 1(a) and (b).

Manuscript received September 21, 2005; revised December 7, 2005.

A. Guermache, V. Voiriot, and R.-M. Capella are with Avanex France, 91625 Nozay, France (e-mail: ali.guermache@wanadoo.fr; Vincent_Voiriot@avanex.com; Rose-Marie_Capella@avanex.com).

P. Gallion is with Ecole Nationale Supérieure des Télécommunications, 75634 Paris, France (e-mail: gallion@enst.fr).

J. Jacquet is with Supelec, Laboratoire Matériaux Optiques, Photonique et Systèmes (LMOPS), 57070 Metz, France (e-mail: Joel.Jacquet@metz.supelec.fr).

Digital Object Identifier 10.1109/LPT.2006.871640

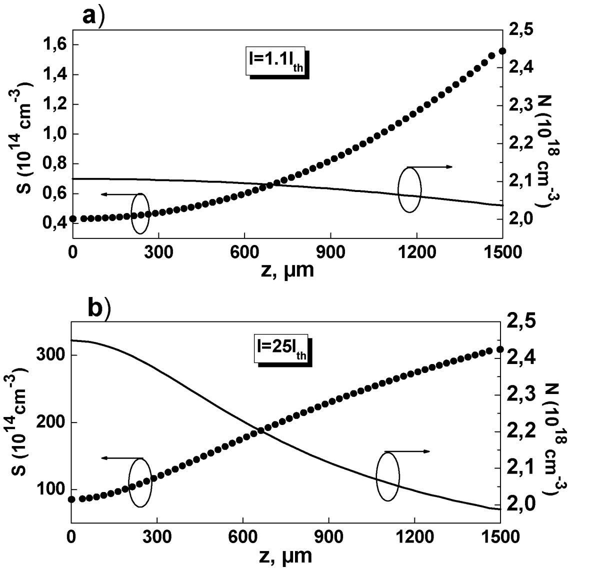

Fig. 1. Photon (•) and carrier (solid line) density profiles calculated for (a) $I \cong I_{\text{threshold}}$ and (b) $I = 25 I_{\text{threshold}}$.

This illustrates that the cavity has a different behavior between threshold and high current injection. The same remark suits for carrier distribution along the cavity [right scale of Fig. 1(a) and (b)].

We observe in these figures, that the carrier density at the front facet ($z = 1500$) is reduced due to the increase of the photon density. This implies an increase at the rear facet ($z = 0$) of the carrier density to maintain the threshold condition (e.g., the averaged round-trip gain equals the total losses). The same scale is used for Fig. 1(a) and (b) to represent the carrier density distribution $N(z)$. This allows us to show the enhancement of the carrier distribution asymmetry between threshold [Fig. 1(a)] and $25 \times I_{\text{threshold}}$ [Fig. 1(b)]. The factor $(N_{z=0}/N_{z=1500})$, that represents this asymmetry is increased by 20% from 1.04 at threshold [Fig. 1(a)] to 1.24 at $25 \times I_{\text{threshold}}$ [Fig. 1(b)].

In order to limit this asymmetry at the origin of the power saturation [8], we design structures for which the photon density is kept constant along the active stripe. Equation (3) summarizes this condition

$$\frac{S(z)}{W_{\text{mode}}(z)} = \frac{S(0)}{W_{\text{mode}}(0)} \tag{3}$$

where $S(z)$ and $W_{\text{mode}}(z)$ are the calculated photon density profile and the mode width [full-width at half-maximum (FWHM)] at a distance z from the reverse facet ($z = 0$), respectively.

In addition, we calculate the FWHM for the fundamental mode as a function of the waveguide width for a straight cavity. This optical mode calculation leads to a linear behavior of the fundamental mode size versus stripe width

$$W_{\text{mode}}(z) = aW_s(z) + b \tag{4}$$

where W_s is the stripe width, and a and b are constant.

From (3) and (4), we can determine the complete evolution of the slightly flared stripe width along the cavity. The results of the calculated stripe width along the 1500-μm cavity are plotted in Fig. 2, for the two different structures corresponding to Fig. 1(a) and (b): Structure_I_{th} is designed to give uniform photon density at threshold current and Structure_$25I_{\text{th}}$ at $25 \times I_{\text{threshold}}$. At low current, the LSHB impact on gain saturation and carrier density profile is still low. Waveguide of Structure_I_{th} can, therefore, be approximated by an exponential function. At the opposite, Structure_$25I_{\text{th}}$ calculated for high current injection is much better fitted with a polynomial function. We used the results of this calculation to draw the mask that has been used in the process.

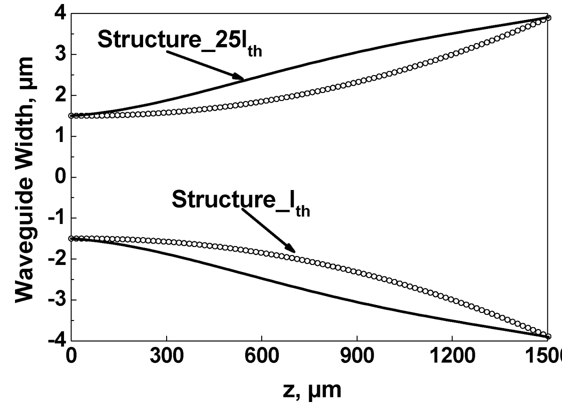

Fig. 2. Calculated waveguide width for Structure_I_{th} (∘) and Structure_$25I_{\text{th}}$ (solid line).

III. Device Fabrication

The structure is an InGaAsP–InP buried ridge waveguide. The gas source molecular beam epitaxy grown active layers consist of five compressively strained InGaAsP quantum wells separated by four lattice-matched barriers. The active layer is sandwiched between two nonintentionally doped 1.17-μm InGaAsP separate confinement layers. The photoluminescence peak is centered at 1470 nm. Selective growth is then performed to realize p-n InP blocking layers on both sides of the dry etched mesa. The ridge is then buried with optimized p-doping profile InP cladding and InGaAs p++ contact layers. Then, metallic contact layers are deposited on both the p- and n-sides. The wafer is cleaved into bars of 1500 μm, where straight and flared lasers are alternatively localized, allowing simultaneous facets coating. The front and rear facets are coated with 3% and 95% reflectivity mirrors, respectively. The laser chips are p-side down mounted onto AlN submonts and placed on a copper heatsink. All continuous-wave (CW) measurements were done with thermal control of the copper heatsink.

IV. Results and Discussion

Comparison of standard experimental electrooptic parameters of flared and straight waveguides are summarized in Table I. The threshold current is an increasing function of the waveguide surface (current injection area); this leads to a quasi-constant current threshold density for the three structures.

At the opposite, the series resistance decreases when the waveguide area increases. This resistance reduction is due to the larger area provided by both flared structures in comparison

TABLE I
STANDARD EXPERIMENTAL PARAMETERS RESULTS

Design	I_{th} (mA)	J_{th} (kA/cm^2)	η (W/A)	R_s (Ω)
Straight waveguide	29	0.64	0.41	1.09
Structure_I_{th}	43	0.63	0.42	0.86
Structure_25I_{th}	48	0.60	0.41	0.76

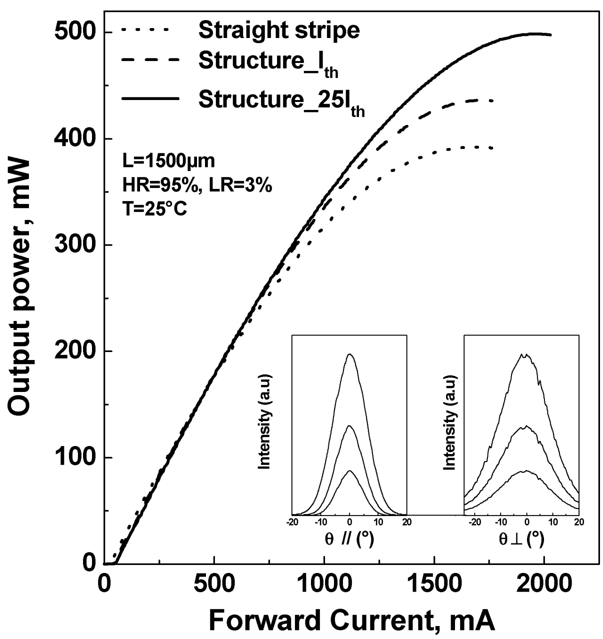

Fig. 3. Output power as a function of current intensity under CW operation at $T = 25$ °C, for straight laser (●), Structure_$I_{\rm th}$ (— — —), and Structure_$25I_{\rm th}$ (solid line). Inset: Far-field patterns of Structure_$25I_{\rm th}$ for parallel and perpendicular plane, current values are 0.05, 0.2, and 0.8 A.

with the straight active waveguide. All these results are in agreement with predictions.

The flared waveguide optimized at threshold Structure_$I_{\rm th}$ shows actually a slightly better external efficiency and the Structure_$25I_{\rm th}$ has the same slope efficiency as the straight stripe. Both structures do not exhibit degradation in the slope efficiency; this confirms that slightly flared stripes do not provide excess losses. Fig. 3 shows output power versus current characteristics for each structure from the same wafer under CW operation at room temperature ($T = 25°$C). As it can be seen, a maximum output power (500 mW) is obtained for the slightly flared Structure_$25I_{\rm th}$, for a current of $I = 1.9$ A. This structure demonstrates a better behavior for high current level ($I > 0.7$ A).

These results were expected as LSHB increases with increasing current. For high current level, an important photon density near the front facet is reached leading to local gain saturation effect. Structure_$25I_{\rm th}$, optimized for high current level, provides a better resistance against LSHB effect.

The inset of Fig. 3 shows far-field patterns of the Structure_$25I_{\rm th}$ for different currents. Single transverse mode behavior is obtained up to $I = 0.8$ A. The beam divergence is $13° \times 20°$ in the parallel and perpendicular planes, respectively.

V. CONCLUSION

We have demonstrated that by a novel design of flared waveguides, we can reduce the carrier and photon profiles inhomogeneity along a 1480-nm pump laser cavity. In such optimized structure, the effect of gain saturation is limited and an improvement of the output power is obtained. Experimental comparison between straight and flared devices confirms our design rules. The best flared stripe shows 500-mW-high output power at 1.9 A compatible with Raman amplification. This result corresponds to a 30% output power improvement for the flared stripe compared to the straight one. Single transverse mode behavior without astigmatism is also obtained with the flared cavity, allowing a simple coupling scheme with two lenses only.

REFERENCES

[1] D. Garbuzov, A. Komissarov, I. Kudryashov, M. Maiorov, R. Roff, and J. Connolly, "High power Raman pumps based on ridge waveguide in InGaAsP/InP diode lasers," in *Proc. Opt. Fiber Communication Conf.*, 2003, pp. 394–396.

[2] S. Delepine, F. Gerard, A. Pinquier, T. Fillion, J. Pasquier, D. Locatelli, J.-P. Chardon, H. K. Bissessur, N. Bouche, F. R. Boubal, and P. Salet, "How to launch 1 W into single-mode fiber from a single 1.48-μm flared resonator," *IEEE J. Sel. Topics Quantum Electron.*, vol. 7, no. 2, pp. 111–123, Feb. 2001.

[3] K. Hamamoto, K. Naniwae, and M. Ohya, "High power with low electric power consumption active multi-mode interferometer laser diode for fiber amplifier," *Electron. Lett.*, vol. 38, no. 11, pp. 517–519, 2002.

[4] D. F. Welch, P. S. Cross, D. R. Scifres, W. Streifer, and R. D. Burnham, "High power, AlGaAs buried heterostructure lasers with flared waveguides," *Appl. Phys. Lett.*, vol. 50, no. 2, pp. 233–235, 1987.

[5] M. Sagawa, K. Hiramoto, T. Toyonaka, T. Kikawa, S. Fujisaki, and K. Uomi, "Highly reliable and stable lateral mode operation of high power 0.98 μm InGaAs-InGaAsP lasers with an exponential shaped flared stripe," *IEEE J. Sel. Topics Quantum Electron.*, vol. 3, no. 2, pp. 666–671, Feb. 1997.

[6] R. B. Swint, A. E. Huber, T. S. Yeoh, C. Y. Woo, J. J. Coleman, B. O. Faircloth, and M. S. Zediker, "650 mW single lateral mode power from tapered and flared buried ridge laser," *IEEE Photon. Technol. Lett.*, vol. 14, no. 9, pp. 1237–1239, Sep. 2002.

[7] F. Rinner, J. Rogg, P. Friedmann, M. Mikulla, R. Propawe, and G. Weimann, "Longitudinal carrier density measurement of high power broad area laser diodes," *Appl. Phys. Lett.*, vol. 80, pp. 19–21, 2002.

[8] A. Guermache, V. Voiriot, D. Locatelli, F. Legrand, R.-M. Capella, P. Gallion, and J. Jacquet, "Experimental demonstration of spatial hole burning reduction leading to 1480-nm pump lasers output power improvement," *IEEE Photon. Technol. Lett.*, vol. 17, no. 10, pp. 2023–2025, Oct. 2005.

[9] H. Bissessur, "Effects of hole burning, carrier-induced losses and the carrier-dependent differential gain on the static characteristic of DFB lasers," *J. Lightw. Technol.*, vol. 10, no. 11, pp. 1617–1630, Nov. 1992.

[10] G. Björk and O. Nilsson, "A new exact and efficient numerical matrix theory of complicated laser structures: Properties of asymmetric phase shifted DFB lasers," *J. Lightw. Technol.*, vol. LT-5, no. 1, pp. 140–146, Jan. 1987.